Applied Catalysis B: Environmental 251 (2019) 273–282

Contents lists available at ScienceDirect

Applied Catalysis B: Environmental

journal homepage: www.elsevier.com/locate/apcatb

Heterogeneous activation of peroxymonocarbonate by chalcopyrite ($CuFeS_2$) for efficient degradation of 2,4-dichlorophenol in simulated groundwater

Xiangjian Xu[a,b], Dingding Tang[a], Jianhua Cai[a], Beidou Xi[b,*], Yan Zhang[a], Liu Pi[a], Xuhui Mao[a,*]

[a] School of Resource and Environmental Science, Hubei International Scientific and Technological Cooperation Base of Sustainable Resource and Energy, Wuhan University, Wuhan, 430072, China

[b] State Key Laboratory of Environmental Criteria and Risk Assessment, Chinese Research Academy of Environmental Sciences, Beijing, 100012, China

ARTICLE INFO

Keywords:
$CuFeS_2$
Peroxymonocarbonate
Heterogeneous activation
2,4-Dichlorophenol
Fenton

ABSTRACT

Recently, increasing attention has been paid to the activated peroxymonocarbonate (APMC) process, because it is envisioned to be engineered for the chemical oxidation remediation of groundwater in karstic regions with elevated levels of naturally occurring bicarbonate. In the present study, we explored the feasibility of using metal sulfides ($CuFeS_2$, CuS, and FeS_2) as the catalysts for heterogeneous APMC (H-APMC) processes. Among the three synthesized metal sulfides, the $CuFeS_2$ catalyst exhibited reversible redox properties, thereby it had the best performance to activate peroxymonocarbonate (PMC) for the degradation of 2,4-dichlorophenol (2,4-DCP). The X-ray photoelectron spectroscopy analysis and density-functional-theory calculations both revealed that, for the $CuFeS_2$-catalyzed APMC process, iron sites of $CuFeS_2$ acted as the catalytic active sites. Electron spin resonance and chemical quenching experiments revealed that the intermediated reactive species for a $CuFeS_2$-catalyzed APMC process included hydroxyl radicals ($^{\cdot}OH$), singlet oxygen ($^1O_2$), superoxide radicals ($^{\cdot}O_2^-$), and carbonate radicals ($^{\cdot}CO_3^-$). It was also found that, under a low bicarbonate condition (≤ 25 mM), the concentration of H_2O_2 was not the limiting factor that controlled the degradation rate of 2,4-DCP. Instead, bicarbonate concentration and catalyst dosage significantly influenced the performance of $CuFeS_2$-catalyzed APMC process. Al_2O_3-supported $CuFeS_2$ catalyst (Al_2O_3@$CuFeS_2$) was prepared and tested as fillers for practical application. The flowing experiment using fixed-bed reactor showed that the Al_2O_3@$CuFeS_2$ fillers could effectively activate PMC and thereby degraded the 2,4-DCP. Runoff of the coated $CuFeS_2$ component occurred during the experiment, but the leached copper and iron species from the fillers were constantly at a low and safe level (< 1.5 mg/L). The $CuFeS_2$-catalyzed APMC process showed a good prospect for groundwater remediation in karstic regions.

1. Introduction

In-situ chemical oxidation (ISCO) is an effective technology for the remediation of contaminated soil and groundwater due to its advantages such as easy operation, high efficiency and saving time [1,2]. Various kinds of oxidizing agents such as permanganate, ozone, hydrogen peroxide (H_2O_2), activated persulfate have been used for the cleanup of organic compounds in groundwater [3–5]. However, the performances of these oxidants are greatly influenced by the characteristics of contaminated sites. For example, for groundwater in karstic aquifers, carbonate dissolution leads to the presence of elevated bicarbonate (HCO_3^-) concentration in liquid phase [6–9], and bicarbonate concentration was reported to reach as high as ten millimoles per liter in some karstic regions [7,8,10–12]. The existence of bicarbonate in groundwater may attenuate the chemical oxidation of pollutants in an ISCO process. For the remedial operation using H_2O_2 and ferrous salts, the weakly alkaline pH of bicarbonate-containing groundwater is not good for maximizing the performance of Fenton reaction, and bicarbonate ions also had scavenging effect on oxidizing hydroxyl radicals [13,14].

Recently, utilizing activated peroxymonocarbonate (APMC) for the abatement of organic pollutants has drawn more attentions for its high oxidation efficiency under weakly alkaline conditions [13,15–19]. The APMC process can generate reactive species including hydroxyl radicals ($^{\bullet}OH$), superoxide radicals ($^{\cdot}O_2^-$) and singlet oxygen ($^1O_2$) for the oxidation of organics [15,18,20]. Different from the Fenton reaction

* Corresponding authors.
E-mail addresses: xibeidou@yeah.net (B. Xi), clab@whu.edu.cn (X. Mao).

https://doi.org/10.1016/j.apcatb.2019.03.080
Received 11 December 2018; Received in revised form 17 March 2019; Accepted 30 March 2019
Available online 01 April 2019

that maximizes its performance under very acidic condition, APMC process works under near-neutral or alkaline conditions. Therefore, it is envisioned to be developed as a chemical oxidation technology for the remediation of contaminated groundwater in karstic regions. Peroxymonocarbonate (PMC) rapidly forms in the aqueous mixture of bicarbonate and H_2O_2 according to the chemical equilibrium below:

$$HCO_3^-(aq) + H_2O_2(aq) \leftrightarrow HCO_4^-(aq) + H_2O;\ K_{eq} = \frac{[HCO_4^-]}{[H_2O_2][HCO_3^-]} \quad (1)$$

The equilibrium constant (K_{eq}, 0.33 M^{-1} in water at 25 °C) suggests that PMC is basically at a low level in the mixture relative to the H_2O_2 and bicarbonate. Nevertheless, PMC can be further activated by some metallic catalysts, such as metal ions cobaltous ions (Co^{2+}), copper ions (Cu^{2+}) and ferrous ions (Fe^{2+}), to achieve more efficient oxidation of organic pollutants [13,15,16,18]. It has been reported that the APMC process could greatly accelerate the degradation of triclosan [18], amino acids [21], olefins [22,23], and organic dyes [17]. So far, cobaltous ions stand out as the most efficient catalyst for APMC process [13,15,21]. However, the toxicity of cobaltous ions greatly limits its prospect for practical application in environmental remediation. Alternatively, using Co-based heterogeneous catalysts for APMC process can avoid the direct use of Co^{2+} ions. Researchers reported the efficient degradation of organic pollutants by heterogeneous APMC (H-APMC) process using Co-bearing catalysts, such as Co-intercalated layered double hydroxides and Co-Mn spinel oxides [19,24]. Although these catalysts showed good performances on activating PMC for the oxidative degradation of organic pollutants, the environmental risk of cobalt release still existed.

Transition metal sulfides (TMS) are the most abundant natural sulfur minerals on the earth's surface and often found in metal ore and coal mines. TMS have been tested as catalysts for some chemical oxidation processes. FeS_2 was reported to act as a heterogeneous catalyst for Fenton reactions, and it also showed the capability to activate persulfate for decontamination under acidic pH conditions [25]. In addition to FeS_2, Mi et al. [26] reported that three-dimensional copper sulfide (CuS, covellite) catalysts exhibited good performance for activating hydrogen peroxide for the oxidative degradation of methylene blue and rhodamine. Oturan et al. [27] demonstrated the utilization of chalcopyrite ($CuFeS_2$) as the heterogeneous catalysts for electrochemical advanced oxidation process, in which chalcopyrite catalysts showed impressive activity for the degradation of antibiotic tetracycline. TMS are readily available mineral materials that have transition metal reactive sites, and they are more reducing and reactive than the corresponding metal oxides. Therefore, from the perspectives of engineering application, it is worth of exploring the feasibility of using TMS for H-APMC process.

In the present study, we prepared three TMS materials, including FeS_2, CuS and $CuFeS_2$, and investigated their performances on activating PMC for the degradation of 2,4-chlorophenol (2,4-DCP). 2,4-DCP was selected as the model pollutant because chlorophenols were reportedly detected at the levels of up to ten ppm in the groundwaters and aquifers of some contaminated sites [28,29]. These three TMS were selected because they were readily available minerals and did not contain the toxic cobalt element. The catalytic activities of these materials for H-APMC oxidizing systems were investigated first, and then the activating mechanism of TMS for PMC was accordingly studied. In addition to the batch experiments, the long-term stability of the catalysts for H-APMC process was evaluated in a fixed-bed column reactor. The results showed that the $CuFeS_2$-activated PMC process could be developed as environmentally friendly technology for decontamination under pH conditions close to those of natural waters, especially for the contaminated karst regions with naturally occurring bicarbonate.

2. Materials and methods

2.1. Chemicals

Ethylene glycol, tert-butyl alcohol (TBA) and 5,5-dimethyl-1-pyrroline N-oxide (DMPO) were purchased from the Aldrich company. Other chemicals including ferric chloride, cuprous chloride, ammonium sulfide, ferrous chloride, cupric nitrate, thiourea, ethanol, methanol, 2,4-dichlorophenol, hydrogen peroxide (30%, w/w), sodium bicarbonate, sodium azide (NaN_3), p-benzoquinone (BQ) was obtained from the Shanghai Sinopharm Chemical Reagent Co., Ltd. All of the reagents used were of analytical reagent grade and were used without further purification. All the aqueous solutions were prepared using deionized water throughout the experimental procedure and analyses.

2.2. Preparations of metal sulfides and Al_2O_3-supported $CuFeS_2$

FeS_2 was prepared by a simple solvothermal method according to the reference [30]. Typically, 10 mmol of ferrous chloride was dissolved into 80 mL of ethylene glycol, followed by the addition of 30 mmol of thiourea at room temperature. After being stirred vigorously for 30 min, the resultant mixture was transferred to a 100 mL Teflon-lined stainless steel autoclave for hydrothermal reaction at 160 °C for 12 h. The product was collected by centrifugation, washed with ethanol and deionized water three times, and then dried in vacuum at 80 °C. Similar method as above was used to prepare CuS followed by using cupric nitrate instead of ferrous chloride.

$CuFeS_2$ was synthesized by the hydrothermal reaction method [31,32]. For example, solutions of cuprous chloride (5.04 mmol) and ferric chloride (5.04 mmol) were mixed well into 80 mL of ethylene glycol and then followed by the addition of 10.2 mmol of ammonium sulfide. After being stirred vigorously for 30 min, the resultant mixture was transferred to a 100 mL Teflon-lined stainless steel autoclave for hydrothermal reaction at 200 °C for 10 h. Then, the solution was cooled to room temperature, and the resultant solid product was collected by centrifugation, washed with ethanol and deionized water three times, and dried in vacuum at 80 °C. All the products were stored in a desiccator for further analysis and experiments.

Al_2O_3-supported $CuFeS_2$ catalyst for the fixed-bed experiment was also prepared via the hydrothermal reaction method. In addition to the reaction solution, γ-Al_2O_3 fillers with 2.5 mm diameter were added into the 100 mL Teflon-lined stainless steel autoclave for hydrothermal reaction at 200 °C for 10 h. Afterwards, the autoclave was cooled to room temperature, and the resultant Al_2O_3-supported $CuFeS_2$ products were collected, washed with ethanol and deionized water three times, and dried in vacuum at 80 °C.

2.3. Batch degradation experiments

The degradation experiments were performed in 140 mL batch reactors with polytetrafluoroethylene (PTFE)-coated butyl rubber septa at 25.0 ± 2 °C. Predetermined amounts of $NaHCO_3$ (e.g., 1.26 g) and H_2O_2 (30%) (e.g., 3.1 mL) were mixed in 100 mL aqueous solution, which was denoted as Solution A. Prior to the reactions, 1.0 mL of 2,4-DCP stock solution (1.0 g/L) was added into the reactors and mixed with 89 mL deionized water. The reaction was then initiated by adding Solution A and 5.0 mg catalysts to the reactor. The reactor was placed on a water bath shaker at 200 rpm for 120 min (25 °C) (see Fig. S1 in the Supplementary materials (SM)). At regular time intervals, 1.0 mL aqueous sample was collected by syringe, filtered immediately via 0.45 μm filter, and transferred into a 2 mL vial, which was prefilled with 1.0 mL of methanol to quench the oxidation reaction. All experiments were carried out in duplicate, and mean values with standard deviations were reported. In order to identify the intermediated reactive species in

the oxidation system, additional experiments were conducted using radical scavengers. Quenching experiments were conducted with the addition of TBA, NaN_3 and BQ, which were widely employed as radical scavengers for •OH, $^1O_2$ and $•O_2^-$, respectively.

2.4. Degradation experiments using fixed-bed column reactor

Degradation of 2,4-DCP was investigated in a fixed-bed column reactor filled with Al_2O_3-supported $CuFeS_2$ catalysts. The column reactor was made of glass, with a dimension of 15 cm height and 5 cm inner diameter (see Fig. S2 in the SM). Approximately 70 g Al_2O_3-supported $CuFeS_2$ catalysts were used to pack the column with a pore volume (PV) of 50 mL. A peristaltic pump (BT100-2 J, Longer Precision Pump Co., Ltd., China) was used to feed the reaction solution from the inlet at a constant flow rate of 1.67 mL/min (30 min residence time). The reaction solution consisted of 10 mg/L 2,4-DCP, 15 mM $NaHCO_3$, and 30 mM H_2O_2. Prior to the experiment, deionized water was pumped to the column to remove air bubbles and ensure uniformity. Samples were withdrawn at different intervals and filtered through 0.45 μm membrane for analysis.

2.5. Analytical and characterization methods

The concentration of 2,4-DCP was measured using a High-Performance Liquid Chromatography (HPLC) consisting of a Shimadzu 15C HPLC pump and a UV/Visible detector at 220 nm. The mobile phase was a mixed methanol and water solution (70:30, v/v), and the flow rate was 1.0 mL/min. The degradation intermediates of 2,4-DCP were measured using an Agilent liquid chromatograph mass spectrometer (LC−MS, Waters SQD2). The fragments were analyzed via total ion chromatogram (TIC) and ES + scan mode. Total organic carbon (TOC) of reaction solution was determined using a Shimadzu TOC-L CPH CN200 analyzer. FeS_2, CuS and $CuFeS_2$ before and after catalytic reactions were characterized using established methods. X-ray diffraction (XRD) patterns of materials were acquired using a Shimadzu X-ray 600 unit with Cu Kα radiation (40 kV and 40 mA) at a scanning rate of 4°/min. FTIR spectra of materials were recorded in the region 400-4000 cm^{-1} using a Nicolet Avatar 360 spectrometer. The morphologies of the catalysts were examined with a field-emission scanning electron microscopy (SEM; FEI Sirion field emission) and transmission electron microscopy (TEM; FEI Tecnai G2 F30 operating at 300 kV). X-ray photoelectron spectroscopy (XPS) was performed on a photoelectron spectrometer (XSAM800, KRATOS, UK) with monochromatic Mg Kα radiation at 1253.6 eV. Particle size was determined by laser scattering technique on Microtrac S3500. The specific surface areas of FeS_2, CuS and $CuFeS_2$ were calculated based on Brunauer-Emmett-Teller (BET) model. The electrochemical redox properties of as-prepared catalysts in 0.1 M Na_2SO_4 solution were investigated by cyclic voltammetry using electrochemical station CHI 660C. The electrodes were prepared by pressing the precursory slurry (powdered metal sulfides, carbon black and PTFE, with a mass ratio of 8:1:1) onto titanium mesh, and dried at 60 °C. Iron and copper ions concentration were determined using an inductively coupled plasma atomic emission spectrometer (ICP-AES, Perkin Elmer ELAN, DRC-e). Electron spin resonance (ESR) spectra were recorded at room temperature using a Bruker X-band A200 spectrometer with the following parameters: center field 3504 G, sweep width 150 G, microwave frequency 9.82 G, modulation frequency 100 kHz, microwave power 70 mW. 20 μL DMPO was added into 2 mL reaction solution as a spin-trapping agent. The acute toxicity of the effluent from the fixed-bed column was evaluated with a soil dehydrogenase activity assay [33]. This assay is a colorimetric method based on the conversion of 2,3,5-triphenyltetrazolium chloride (TTC) to 1,3,5-triphenylformazan (TPF), and more details can be found in Text S1 in the SM.

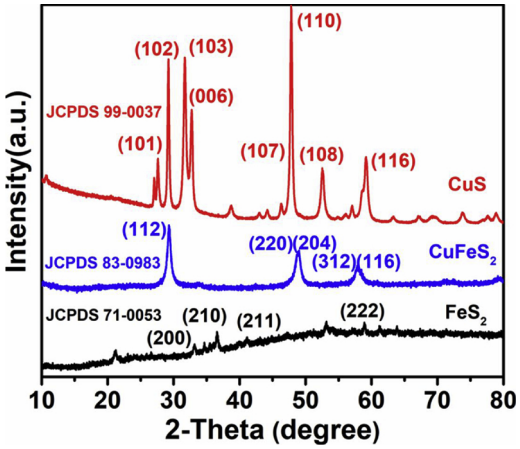

Fig. 1. XRD pattern of the as-prepared FeS_2, CuS and $CuFeS_2$ materials.

2.6. Computational methods

All the density-functional-theory (DFT) calculations were performed by Vienna ab initio simulation package (VASP) on the basis of projector-augmented wave (PAW) method to mainly elucidate the catalytic active centers and the valence changes in the process of HCO_4^- activation by $CuFeS_2$. More details about the DFT calculations are presented in Text S2 of the SM.

3. Results and discussion

3.1. Characterization of the as-prepared metal sulfides

XRD patterns of the as-synthesized metal sulfides are shown in Fig. 1. The characteristic peaks of CuS are clearly observed at 2θ angles 27.7°, 29.2°, 31.7°, 32.8°, 47.9°, 52.6°, and 59.2°. These peaks matched well with the JCPDS data for CuS (JCPDS File no. 99-0037) [34], and the strong intensity of the XRD peaks implied the high crystalline nature of the CuS sample. $CuFeS_2$ exhibits the typical pattern of a tetragonal structure with well-defined peaks occurring at 29.3°, 48.9°, 49.0°, 57.96°, and 58.33°. These peaks corresponded well to the planes of (112), (220), (204), (312), and (116), respectively ($CuFeS_2$, JCPDS NO. 83-0983) [27,35], indicating the high purity of the as-prepared sample. According to the analysis on the solution after synthesis, it was found that the dissolved Fe and Cu species only accounted for 0.1% and 2% of the initially dosed copper and iron, respectively. This observation confirms the successful preparation of $CuFeS_2$. For the FeS_2 sample, all the characteristic diffraction peaks of FeS_2 (JCPDS NO. 71-0053) were detected [36,37]. Meanwhile, some weak impurity diffraction peaks appeared in the pattern, which most likely arose from the partial oxidation of the FeS_2 sample before XRD measurement.

Fig. 2a–k gives the morphologies of the FeS_2, CuS and $CuFeS_2$ samples. As can be observed, the FeS_2 sample exhibited an irregular aggregation of rod-shaped and laminated particles (Fig. 2a, b). The HRTEM image in Fig. 2c exhibits three kinds of lattice fringes with different interplanar distances of ca. 2.34, 2.19 and 1.80 Å, which correspond to the (210), (211) and (221) planes of FeS_2, respectively. By contrast, the CuS particles had a uniform spherical shape, and each microsphere was comprised of many plate-like nanoparticles (Fig. 2d, e). From the TEM image (Fig. 2f) and fast Fourier Transform pattern (Fig. 2g), the lattice fringes and highly symmetric bright spots could be clearly observed. The well-resolved (102), (107), and (108) lattice planes correspond to the spacings of 3.05, 1.95, and 1.78 Å, respectively. $CuFeS_2$ shows a uniform aggregation of spherical nanoparticles, and the nanoparticles were generally in the size range of 10–20 nm

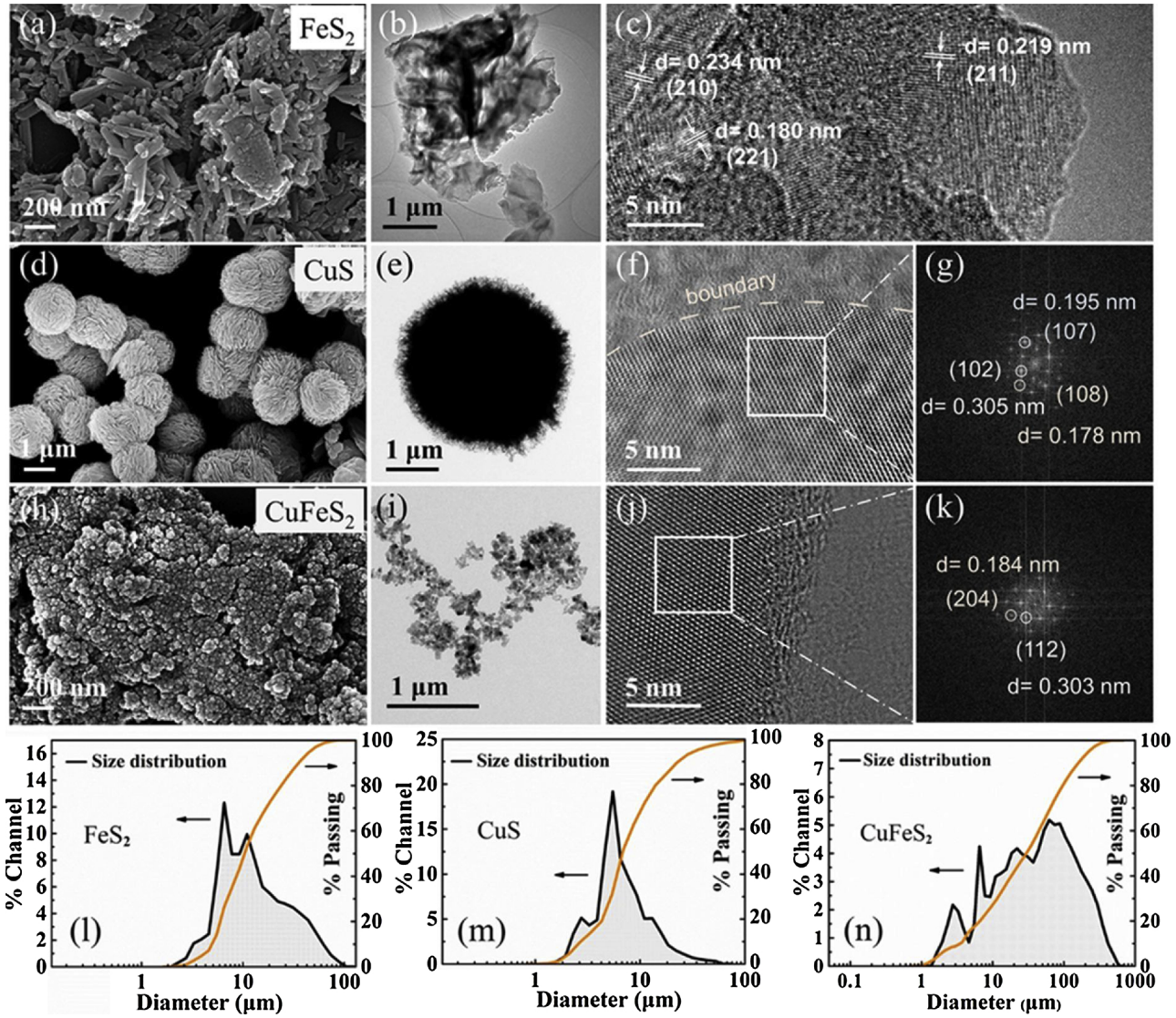

Fig. 2. SEM images of (a) FeS_2, (d) CuS, and (h) $CuFeS_2$. TEM and HRTEM images of (b, c) FeS_2, (e, f) CuS, and (i, j) $CuFeS_2$. Fast Fourier transformation (FFT) images of (g) CuS and (k) $CuFeS_2$, obtained from (f) and (j), respectively. Size distribution of (l) FeS_2, (m) CuS, and (n) $CuFeS_2$.

(Fig. 2h, i). In Fig. 2j, k, the main XRD crystal faces, i.e., (112) and (204) with spacings of 3.03 and 1.84 Å, respectively, could also be identified. In regard to the size distribution, FeS_2 particles display a size distribution ranging from 2 to ~100 μm (Fig. 2l); while CuS (Fig. 2m) showed a narrow size distribution centered at around 6 μm. Compared to the FeS_2 and CuS particles, $CuFeS_2$ had a larger size distribution range centered at around 100 μm (Fig. 2n). Although the $CuFeS_2$ material was composed of tiny nanosized particles, the severe aggregation of the particles did not endow the sample with a huge surface area. BET measurement showed that the specific surface areas of the FeS_2, CuS, and $CuFeS_2$ samples were 3.7 m^2/g, 1.5 m^2/g, and 4.5 m^2/g, respectively. In other words, these three metal sulfides did not show a remarkable difference in surface area.

3.2. 2,4-DCP degradation in H-APMC system

Fig. 3a shows the degradation of 2,4-DCP in $NaHCO_3$ solutions, in heterogeneous Fenton (H-Fenton) systems and in H-APMC systems with the addition of metal sulfides. The catalytic activities of CuS, FeS_2, and $CuFeS_2$ were compared in the three systems. No significant decrease in 2,4-DCP concentration was observed in the presence of $NaHCO_3$, suggesting that the contribution from adsorption was negligible. The removal efficiencies of 2,4-DCP in H-Fenton systems were 46.2%, 55.7%, and 64.7% for the cases using CuS, $CuFeS_2$ and FeS_2 suspended catalysts after 120 min. This observation accords with the reported research works that metal sulfides could catalyze H_2O_2 for the degradation of organic pollutants [38,39]. For the H-APMC system, CuS and $CuFeS_2$ catalysts showed the activity for efficient degradation of 2,4-DCP. Especially, for the $CuFeS_2$-catalyzed H-APMC ($CuFeS_2$-APMC) process, 91.6% of 2,4-DCP was degraded within 120 min. In other words, with the same $CuFeS_2$ catalyst, the H-APMC process showed a much higher removal efficiency than the H-Fenton process (55.7%), while other two metal sulfides did not show the capability to achieve an enhanced removal of 2,4-DCP in H-APMC system.

pH changes of the reaction processes are shown in Fig. 3b. The $CuFeS_2$-APMC process works under a weakly alkaline environment (pH ~8.5) due to the presence of bicarbonate. In the case of the $CuFeS_2$-catalyzed H-Fenton process, the pH gradually increased to ~5.4 in accompany with the consumption of H_2O_2. In contrast to the H-Fenton system [40], the $CuFeS_2$-APMC process worked at weak alkaline pH but achieved better efficiency for 2,4-DCP removal. Another advantage of the alkaline pH of APMC system is the decreased risk of leached metal ions. According to the measurement on the ions in the reaction solution after two hours, dissolved Cu and Fe species in the solution were

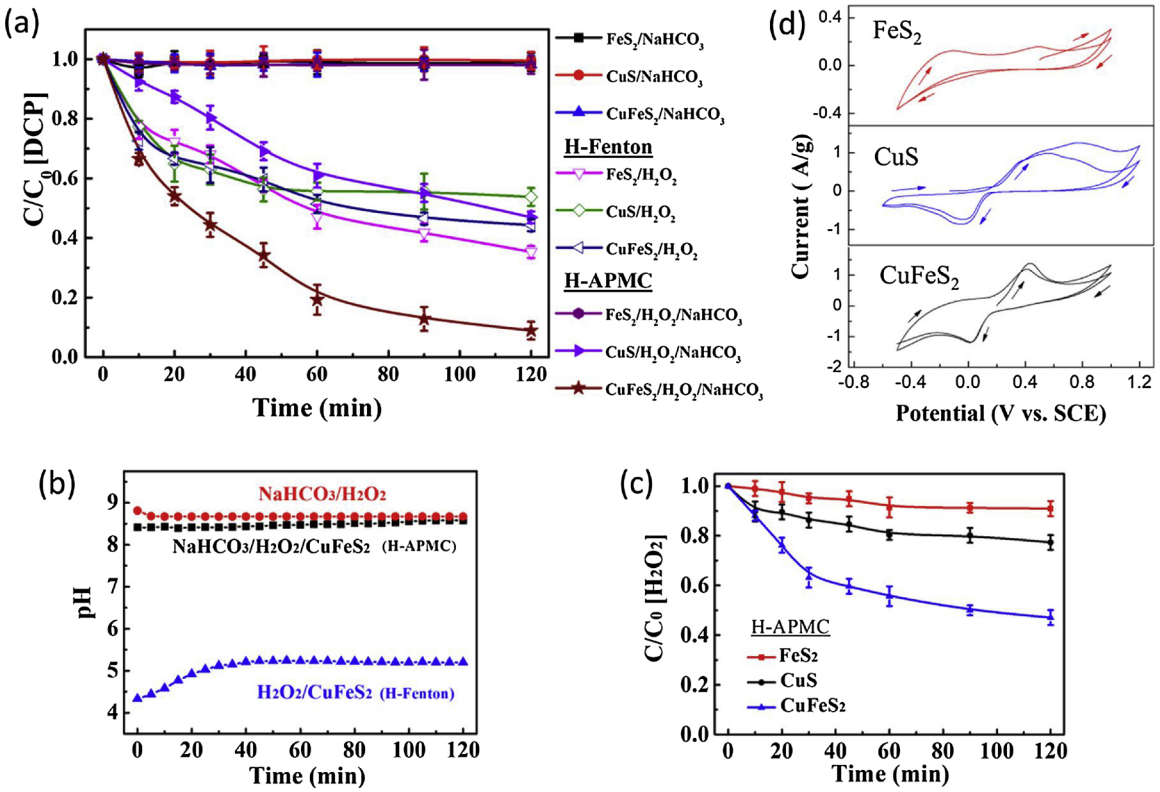

Fig. 3. (a) 2,4-DCP degradation in different heterogeneous catalytic oxidation systems; (b) changes of pH in diff ;erent reaction systems; (c) decomposition of H_2O_2 in the reaction system with different metal sulfide catalysts. Reaction conditions (a, b, and c): [2,4-DCP] = 10 mg/L, [H_2O_2] = 60 mM, [$NaHCO_3$] = 25 mM, and catalyst dosage was 50 mg/L. (d) Cyclic voltammograms of the electrodes using CuS, FeS_2, and $CuFeS_2$ as active materials. The CV measurement was carried out in 0.1 M Na_2SO_4 (pH 8.5) electrolyte at a scan rate of 50 mV/s.

0.056 mg/L and lower than the detection limitation (< 0.01 mg/L), respectively.

In order to reveal the reason for the difference in removal efficiency, the remaining H_2O_2 in the three H-APMC systems were measured (Fig. 3c). The $CuFeS_2$-APMC system demonstrated a faster H_2O_2 decomposition rate than the other two systems. After 2 h of reaction, half the dosed H_2O_2 was remained in the $CuFeS_2$-APMC system, while the decomposition efficiencies of H_2O_2 in the other two systems were 9% (FeS_2) and 23% (CuS), respectively. In the H-APMC system, H_2O_2 is the essential oxidant that drives the various oxidation reactions occurring in the system. A fast decomposition of H_2O_2 means that more reactive radicals formed in the reaction solution and contributed to the oxidation of organic pollutants. The fastest decomposition of H_2O_2 accounted for the best performance of the $CuFeS_2$-APMC system for 2,4-DCP degradation.

Fig. 3d depicts the CV curves of the as-prepared FeS_2, CuS, and $CuFeS_2$ electrodes in alkaline Na_2SO_4 electrolyte. For the FeS_2 electrode, two oxidation peaks appeared in the curve; and the first peak centered at -0.2 V vs. SCE suggests that FeS_2 was particularly vulnerable to oxidation. However, no well-defined reductive peaks were found in the CV curves of FeS_2. The CuS electrode shows evident oxidative and reductive peaks, however, the oxidative peak had a much larger area than the reductive peak. This unsymmetrical characteristic of the peaks implies that the CuS material might undergo a progressive oxidation process in catalytic oxidation system, which could finally deactivate the CuS material. Relative to the CuS electrode, the $CuFeS_2$ electrode showed oxidative and reductive peaks with an identical area. The symmetry of the redox peaks suggests that the $CuFeS_2$ material can proceed reversible redox reactions, and it has a good stability for catalytic reactions. It is well known that the reversible redox properties of catalytic active sites are very crucial to the efficient work of an advanced oxidation system, such as the recycle of Fe(II)/Fe(III) ions for the Fenton reaction and activated persulfate system [41,42]. Likewise, for the H-APMC system, the reversible redox properties of $CuFeS_2$ favored the continuous decomposition of H_2O_2, while CuS and FeS_2 materials cannot provide remarkable catalytic decomposition of oxidants.

3.3. Catalytic mechanism for the sulfide-catalyzed APMC system

In order to clarify the catalytic mechanism of $CuFeS_2$ for H-APMC process, the $CuFeS_2$ catalyst after reaction was collected and analyzed. Fig. 4a shows that the XRD pattern did not change after the reaction. Fig. 4b,c also reveal that the morphology of the $CuFeS_2$ particles did not show visible change, suggesting that this kind of material was stable in the APMC system. The FTIR spectra of $CuFeS_2$ particles before and after use (shown in Fig. S3 in the SM) only shows enhanced signals at 1623 cm^{-1} (stretching vibration of C=O) and 1384 cm^{-1} (deformation vibration of C–H). By contrast, the powdered FeS_2 catalyst showed a significant change in XRD pattern and appearance (see Fig. S4a, b in the SM). The sample was oxidized into crystallized FeO(OH) and the color of powder changed from brown to black. For the CuS sample, its XRD pattern and appearance were basically kept after the reaction (see Fig. S5a in the SM)). The results of XRD analysis and visible inspection are consistent with the CV results that $CuFeS_2$ and CuS were more stable than FeS_2 in the PMC oxidizing environment.

The XPS spectra of the $CuFeS_2$ samples before and after reaction are given in Fig. 4d,e. As can be observed, the binding energy at 932.8 eV in fresh $CuFeS_2$ was assigned to Cu 2p3/2 of Cu(I) [43]. No Cu 2p3/2 satellite peak belonging to Cu^{2+} was observed [44], which is in accordance with the reported XPS results of CuS [45]. After the reaction, the valence of Cu(I) did not change, implying that Cu(I) was not the active site for catalytic reaction. For the Fe2p3/2 core-level spectra, the binding energy values occurring at 711.2 eV and 709.2 eV correspond

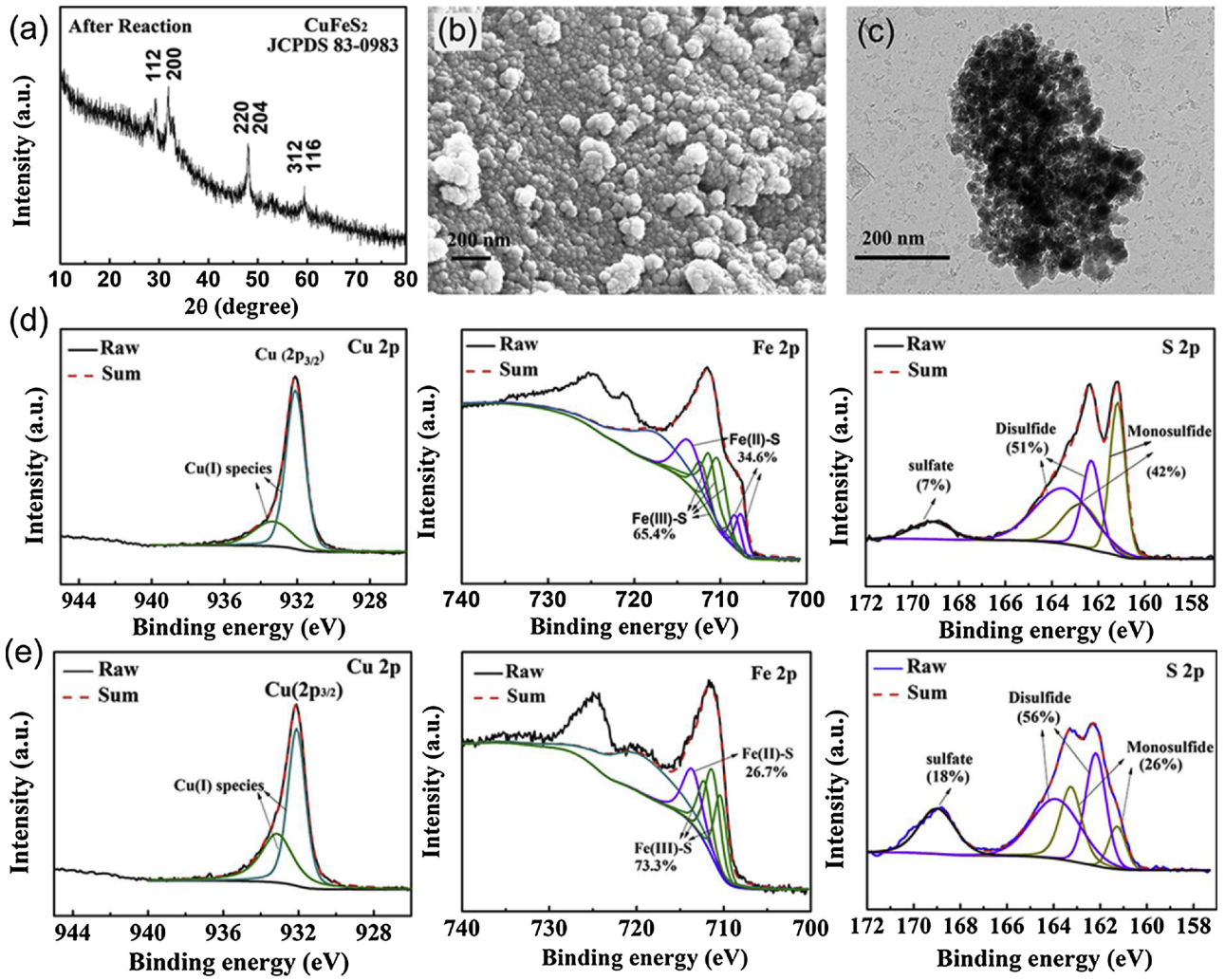

Fig. 4. (a) XRD pattern of the $CuFeS_2$ after reaction; (b) SEM image of the $CuFeS_2$ after reaction; (c) TEM image of the $CuFeS_2$ after reaction. (d) XPS spectra of the pristine $CuFeS_2$ in the region of Cu 2p, Fe 2p, and S 2p; (e) XPS spectra of $CuFeS_2$ after reaction in the region of Cu 2p, Fe 2p, and S 2p.

to ferric iron (Fe(III)) and ferrous iron (Fe(II)), respectively [46]. This observation means that Fe(II)/Fe(III) both existed in the pristine $CuFeS_2$ sample. After the reaction, the relative content of Fe(III) on the surface increased from ~65.4% to ~73.3%, indicating that surface iron atoms are the potential catalytic active sites for APMC process. In the case of the S2p core-level spectral region, the sulfur element existed in the form of sulfate, monosulfide and disulfide, which is in accordance with the previously reported results [47]. After the reaction, the relative content of sulfate increased from ~7% to ~18%. This means that the sulfur element on the surface underwent partial oxidation: the low-valent monosulfide was oxidized into high-valent disulfide and sulfate. For the FeS_2 and CuS catalysts, the XPS analysis showed that, both metal elements (i.e., Fe(II) for FeS_2, and Cu(I) for CuS) and low-valent monosulfide underwent oxidation reactions in the H-APMC system (see Fig. S4 (c–f), and Fig. S5 (c–f) in the SM). According to the XPS results, the role of sulfur, iron and copper can be further analyzed. The conversion from low-valent sulphur to sulfate was found for the three samples, while only $CuFeS_2$ showed the capability to efficiently activate PMC. Therefore, low-valent sulphur in sulfide should not be the key component for the activation of PMC.

For the iron and copper elements in $CuFeS_2$, the relative content of Fe(III) increased while the signal of Cu(II) did not appear in the spectra. This phenomenon cannot be explained by the redox potentials of Fe (III)/Fe(II) and Cu(II)/Cu(I) couples in aqueous solutions, which are 0.77 and 0.159 V vs. SHE, respectively. With this in mind, the DFT calculations were conducted to give an in-depth insight into the catalytic mechanism of $CuFeS_2$. According to the XRD results, the optimized unit cell of $CuFeS_2$ crystal (space group $I\bar{4}2d$) is given in Fig. 5a. For the bulk structure, the oxidation states of copper, iron, and sulphur were +1, +3, and -2, respectively [48–50]. In Fig. 5b, the optimized HCO_4^- exhibits a peroxo-like species, i.e., with a 1.491 Å O—O bond. The reconstruction of the surface within the chalcopyrite solid structure can be illustrated by Fig. 5c, d. On the reconstructed chalcopyrite surface, the (001)-S (sulphur terminated) $CuFeS_2$ surface could form disulfide groups (S—S bonds, length ~2.203 Å). This was in line with the S2p XPS results of the pristine $CuFeS_2$ (Fig. 4c), in which both S^{2-} and S_2^{2-} were observed. Meanwhile, the presence of S_2^{2-} enabled the formation of Fe (II) on the reconstructed chalcopyrite surface. The Bader charge analyses in Fig. 5g, h show that the S atoms lost about 1.20 electrons while Fe and Cu gained about 1.17 and 0.03 electrons, respectively, indicating that nearly all the electronic charges were transferred from S to Fe atoms rather than to Cu atoms. Compared to copper ($E_{Cu\ site}$ = -319.39 eV) and sulphur site ($E_{S\ site}$ = -312.22 eV), a lower-energy configuration of the HCO_4^- adsorbed on Fe site ($E_{Fe\ site}$ = -320.26 eV) was observed (see Figs. 5e, f, S6 and Table S1 in the SM), suggesting an easier homolysis of O—O bond of HCO_4^- (i.e., $HCO_4^- \rightarrow {}^*O + {}^*HCO_3^-$). The Bader charge analysis on the HCO_4^--adsorbed Fe site in Fig. 5i, j reveals that 0.30 electrons from Fe atoms were transferred to HCO_4^- (0.27 |e|), Cu atoms (0.02 |e|) and S atoms (0.01 |e|). This observation implies that the Fe site is the dominating catalytic

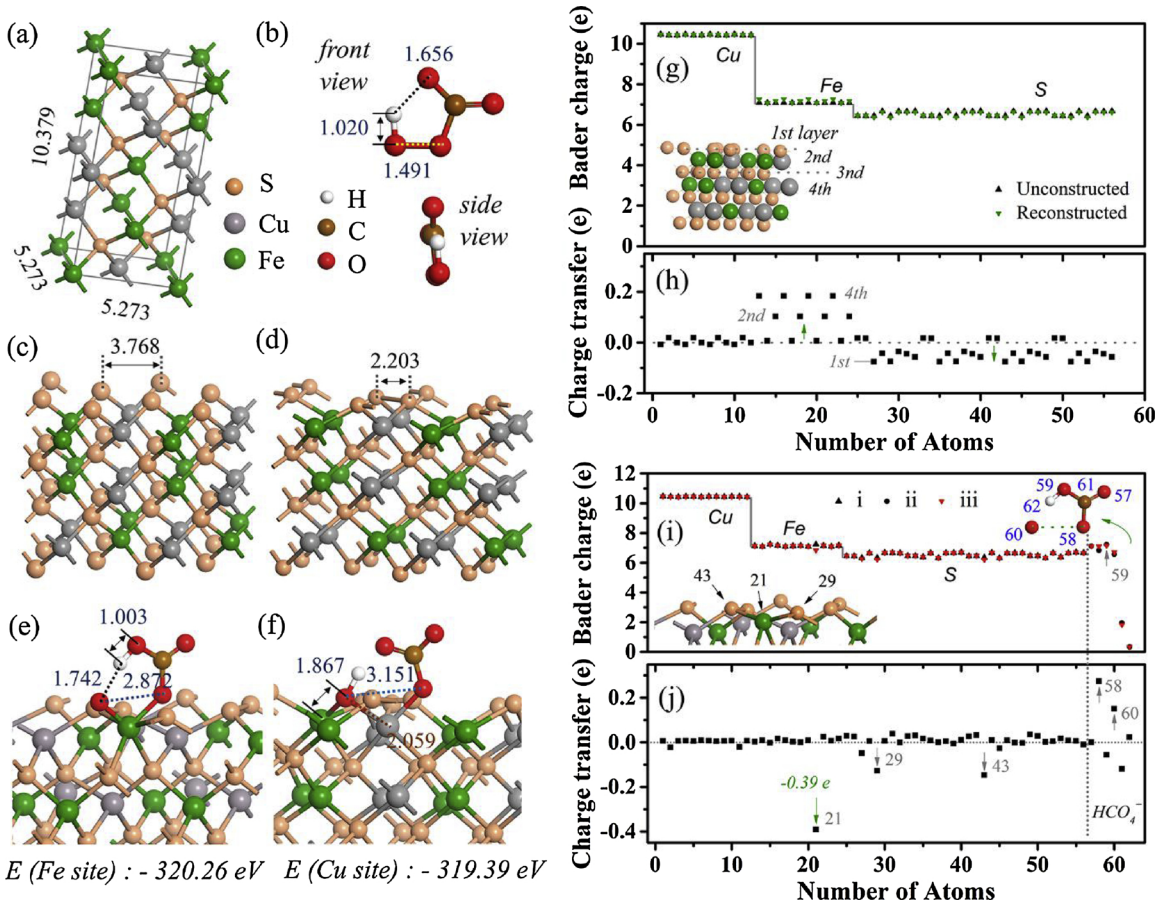

Fig. 5. (a) The optimized unit cell of $CuFeS_2$. (b) Front and side views of the optimized structure of HCO_4^-. Oblique view of (c) the unreconstructed and (d) reconstructed (001)-S chalcopyrite surface. Optimized configurations of the activated HCO_4^- adsorbed on (e) Fe and (f) Cu sites within the (001)-S chalcopyrite substrate. (g) The calculated Bader charges for Cu, Fe, and S atoms in the unreconstructed and reconstructed (001)-S chalcopyrite surface. (i) The calculated Bader charges for Cu, Fe, S, O, C, and H atoms after activation of HCO_4^- by Fe site (*i*, (001)-S surface; *ii*, HCO_4^-; *iii*, the (001)-S surface integrated with HCO_4^-). (h, j) The corresponding charger transfers obtained from (g) and (i), respectively.

active site for activated PMC. After the activation, the oxidized Fe site can be reduced by monosulfide/disulfide, and probably the hydroperoxide in bulk solution [49,50]. As such, the catalytic active sites can be recovered for the functioning of APMC process. It is noted that the calculation results reveal that the $CuFeS_2$ crystal has a good charge transferability (see TDOS and PDOS calculated in Fig. S7 in the SM). This partially accounts for the well-defined CV curves of $CuFeS_2$ (see Fig. 3d).

ESR was employed to probe the reactive oxygen radicals generated in the $CuFeS_2$-APMC system. As displayed in Fig. 6a, no signals of radicals were observed in the control experiments with H_2O_2 alone or in the mixture of H_2O_2 and bicarbonate. In $CuFeS_2$-APMC system, the strong ESR signal with a peak height ratio of 1:2:2:1 could be recognized as the characteristic ESR signal of the DMPO-OH adducts. Moreover, signal of the HDMPO-OH adduct, which has 1:1:1 peak intensities with special hyperfine coupling constants at $\alpha N = 14.7$ G and $\alpha H = 1.1$ G, can be observed [51]. The HDMPO-OH adduct is ascribed to the reaction between the DMPO-OH adduct and the oxidizing species in the system, therefore, the ESR analysis confirmed the contribution of $^{\cdot}OH$ for the degradation of 2,4-DCP.

To better identify the intermediated reactive species contributing to the oxidation of 2,4-DCP, quenching experiments were conducted by spiking the reaction solution ($CuFeS_2$-APMC system) with excessive TBA, NaN_3, BQ and their combinations. TBA, NaN_3, BQ are widely employed as radical scavengers for hydroxyl radicals ($^{\cdot}OH$), singlet oxygen ($^1O_2$) and superoxide radicals ($^{\cdot}O_2^-$), respectively. As shown in Fig. 6b, the degradation of 2,4-DCP was greatly inhibited by adding 2 M TBA, 6 mM BQ or 1.5 mM NaN_3, and the degradation efficiency after 120 min reduced from 79.8%–25.9%, 34.1% and 45.0%, indicating that $^{\cdot}OH$, $^1O_2$ and $^{\cdot}O_2^-$ all contribute to destruction of 2,4-DCP. This observation accords with the reported ROSs found in homogeneous activated-PMC systems [52]. Among three ROS, $^1O_2$ is a selective oxidizing species that shows high reactivity toward electron-rich compounds. When the combinations of different scavengers were added, the removal rates decreased to 16.59%, 23.02%, 32.32% and 9.47% for TBA + BQ, TBA + NaN_3, BQ + NaN_3 and TBA + NaN_3 + BQ, respectively. Even with the combination of three scavengers, the degradation of 2,4-DCP was not completely inhibited. This is probably due to the oxidizing effect of carbonate radicals, which were generated by the activation of PMC, as illustrated by Eq. (2) [53–55].

$$\equiv Fe(II) + 2HCO_4^- \rightarrow \equiv Fe(III) + 2{\cdot}CO_3^- + {\cdot}OH + OH^- \quad (2)$$

Interestingly, $^{\cdot}O_2^-$ signal (DMPO-O_2^-) were not detected during the reaction period, while the quenching experiments indicated the presence of $^{\cdot}O_2^-$. This is probably due to the very short half-life of $^{\cdot}O_2^-$ in protic solvent because it is very sensitive to protons. Following Eq. (2), a series of reactions can occur in the APMC system, resulting in the consumption of H_2O_2 and the degradation of 2,4-DCP. The regeneration of iron active sites on the surface of $CuFeS_2$ can be achieved by Eq. (3), which is important to the continuous functioning of an APMC system. Carbonate radicals ($^{\cdot}CO_3^-$) further react with hydroperoxide, producing $^{\cdot}O_2^-$ and bicarbonate [56]. The resultant $^{\cdot}O_2^-$ from Eqs. (3) and (4) can react with hydroxyl radicals and generate singlet oxygen ($^1O_2$) (Eq. (5)) [57]. As such, 2,4-DCP can be oxidized by

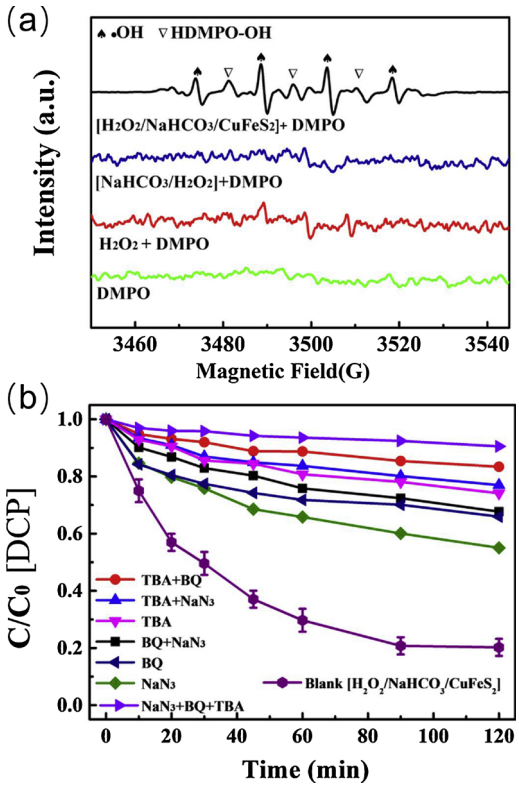

Fig. 6. Identification of the intermediated reactive species in the $CuFeS_2$-APMC system. (a) ESR spectra of the solutions with the addition of DMPO. Experimental conditions are $[NaHCO_3]$ = 15 mM, $[H_2O_2]$ = 30 mM, $[CuFeS_2]$ = 50 mg/L, and [DMPO] =80 mM. (b) Effects of reactive oxygen species scavengers on the degradation of 2,4-DCP with $CuFeS_2$. Experimental conditions included $[NaHCO_3]$ = 15 mM, $[H_2O_2]$ = 30 mM, $[CuFeS_2]$ = 50 mg/L, [2,4-DCP] = 10 mg/L, [TBA] = 2 M, [BQ] = 6 mM, and $[NaN_3]$ = 1.5 mM.

these intermediated reactive species; and the contribution of each species obviously depends on various factors, such as the oxidizing capability and lifetime of the reactive species.

$$\equiv Fe(III) + H_2O_2 \rightarrow \equiv Fe(II) + \bullet O_2^- + H^+ \quad (3)$$

$$\bullet CO_3^- + H_2O_2 \rightarrow HCO_3^- + \bullet O_2^- + H^+ \quad k = 8.0 \times 10^5 M^{-1}s^{-1} \quad (4)$$

$$\bullet O_2^- + \bullet OH \rightarrow {}^1O_2 + OH^- \quad k = 1.01 \times 10^{10} M^{-1}s^{-1} \quad (5)$$

According to the TOC analysis, after 2 h of oxidation reaction in the $CuFeS_2$-APMC system (i.e., $[H_2O_2 + NaHCO_3 + CuFeS_2]$ in Fig. 6b), the TOC of the 2,4-DCP solution was decreased by 53%. The degradation intermediates detected by the LC–MS analysis include 1,2-benzenediol superoxide radical (*m/z* 142.1), parachlorophenol superoxide radical (*m/z* 159), maleic acid (*m/z* 115.1) and oxalic acid (*m/z* 91.1) (see Fig. S8a-c in the SM). Therefore, an oxidative degradation pathway in association with the aforementioned oxidative intermediates can be proposed (see Fig. S8d) for the removal of 2,4-DCP in the $CuFeS_2$-APMC reaction system. Based on the above discussion, we know that reactions in $CuFeS_2$-APMC oxidizing system appear to be more complex than the heterogeneous Fenton system. The presence of bicarbonate in H_2O_2 solution not only altered the routes for •OH generation, but also enriched the reactive species for 2,4-DCP degradation (e.g., singlet oxygen found in the system). The quenching experiments showed that •OH is not a dominating reactive species in the APMC system, but remarkable degradation of 2,4-DCP was still achieved in this weakly alkaline oxidizing system.

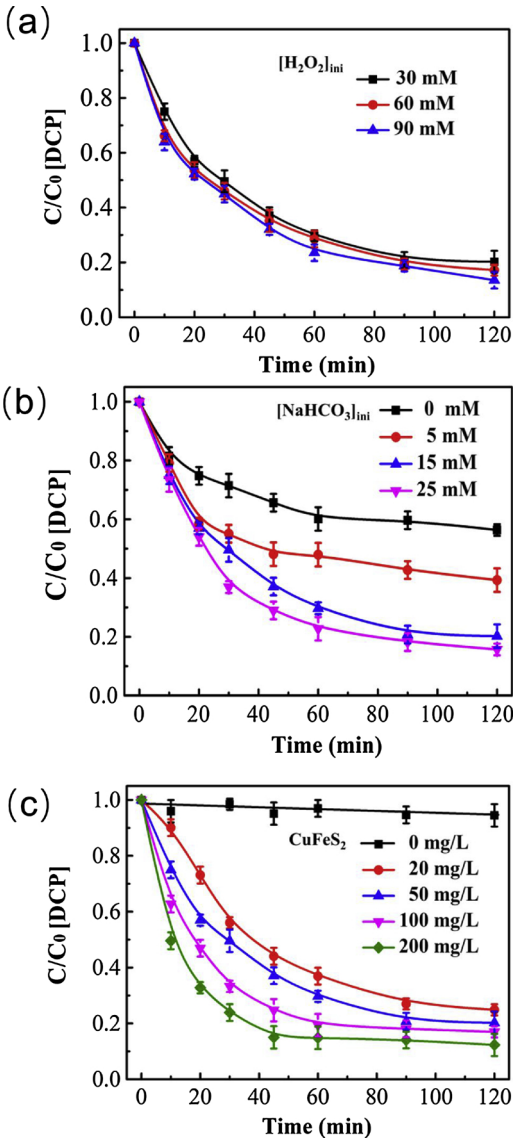

Fig. 7. (a) Effect of initial H_2O_2 concentration ($[H_2O_2]_{ini}$) on 2,4-DCP degradation in $CuFeS_2$-APMC system ($[NaHCO_3]$ = 15 mM, and 50 mg/L $CuFeS_2$). (b) Effect of initial HCO_3^- concentration ($[HCO_3^-]_{ini}$) on the degradation of 2,4-DCP ($[H_2O_2]$ = 30 mM, and 50 mg/L $CuFeS_2$). (c) Decomposition of 2,4-DCP by the APMC system with different $CuFeS_2$ dosages from 0 to 200 mg/L ($[H_2O_2]$ = 30 mM and $[NaHCO_3]$ = 15 mM). [2,4-DCP] = 10 mg/L for all trials.

3.4. Impact of initial H_2O_2 concentration, HCO_3^- concentration and $CuFeS_2$ dosage

Fig. 7a shows the effect of initial H_2O_2 concentration ($[H_2O_2]_{ini}$) on the removal of 2,4-DCP. It reveals that an elevated H_2O_2 concentration did not significantly influence the removal of 2,4-DCP. When the initial H_2O_2 concentration increased from 30 to 90 mM, the removal efficiency of 2,4-DCP after 2 h was only improved by 6.7%. According to the measurement on the remaining H_2O_2 (see Fig. 3c), we know that H_2O_2 was not substantially consumed in the H-APMC system with 50 mg/L $CuFeS_2$ catalyst. Therefore, the amount of H_2O_2 was not the limiting factor that controlled the degradation rate of 2,4-DCP. Meanwhile, this observation implied that the heterogeneous Fenton reaction, in association with the interaction between H_2O_2 and $CuFeS_2$, was sluggish in the $CuFeS_2$-APMC system with an alkaline pH. On the contrary, the estimated redox potential of PMC (E^o (HCO_4^-/HCO_3^-)) is 1.8 V vs. SHE [58], which is favorable to the activation of PMC at near-neutral

pH condition. Our DFT calculations in Fig. 4e verified the strong interaction between HCO_4^- and chalcopyrite surface.

The influence of the initial bicarbonate concentration ($[HCO_3^-]_{ini}$) on 2,4-DCP degradation is given in Fig. 7b. Without bicarbonate, 44% of 2,4-DCP was removed by the H-Fenton system consisting of H_2O_2 and $CuFeS_2$. When bicarbonate was added, the removal efficiencies were greatly improved to 61% for 5 mM, 80% for 15 mM and 84% for 25 mM, respectively. Within the studied range, bicarbonate seems to play a more important role than H_2O_2 for the degradation of 2,4-DCP. Bicarbonate is not an oxidant, but more bicarbonate resulted in a higher equilibrium concentration for PMC. Compared to H_2O_2, bicarbonate ions contributed to a series of radical reactions, and they were not essentially consumed during the functioning of APMC process. Therefore, a higher initial bicarbonate concentration always favors the oxidative degradation of 2,4-DCP in the APMC system.

The effect of $CuFeS_2$ dosage on the degradation of 2,4-DCP is given in Fig. 7c. When the dosage of $CuFeS_2$ increased from 20 mg/L to 200 mg/L, the removal rate of 2,4-DCP was accelerated; and the final removal efficiency after 120 min accordingly increased to 87.8% at 200 mg/L $CuFeS_2$ dosage. More $CuFeS_2$ suspended particles provided more catalytic active sites for the activation of PMC. As a result, a higher $CuFeS_2$ dosage offered elevated levels of intermediated reactive species and faster removal of 2,4-DCP. Compared to the cobalt-bearing catalysts reported by other scholars, the $CuFeS_2$ catalyst can achieve similar high degradation efficiency, but with a less dosage (see Table S2 in the SM) [13,19,24,59]. In order to evaluate the reusability of $CuFeS_2$ catalyst, batch experiments with 6 consecutive trials were conducted. As depicted in Fig. S9 in the SM, after 4 times of operation, $CuFeS_2$ still maintained ~70% of the efficiency of the first trial. After the six trials, the performance of $CuFeS_2$ was approximately attenuated by 50%. This observation means that the activity of $CuFeS_2$ gradually decreased during the functioning of APMC process. According to the XPS results, the oxidation Fe(II) and low valent sulphur still occurred for the $CuFeS_2$ catalysts. The dissolution of sulphate in the solution could lead to the destruction of $CuFeS_2$ crystals. As a result, the loss of catalytic active sites rendered the performance attenuation of $CuFeS_2$. Therefore, in order to maximize the performance of $CuFeS_2$-APMC process, the dosage and operation time of $CuFeS_2$ should be cautiously considered.

3.5. Performance of Al_2O_3-supported $CuFeS_2$ in fixed-bed reactor

From the perspective of practical engineering application, use of nanosized or micronsized powders in aqueous solution is restricted by the loss of active substances and the environmental risk of nanosized particles. Therefore, γ-Al_2O_3 spheres with 2.5 mm diameter were selected as the substrate for loading $CuFeS_2$, and the long-term performance of Al_2O_3-supported $CuFeS_2$ catalyst (Al_2O_3@$CuFeS_2$) was investigated in a fixed-bed reactor, as shown in Fig. S2 in the SM. As can be observed from Fig. 8, when the mixture containing H_2O_2, bicarbonate and 2,4-DCP was pumped into the reactor, a complete removal of 2,4-DCP (> 99%) was achieved over the first 10 h of operation (20 PV). After 72 h of running, the removal efficiency of 2,4-DCP in the effluent was 96%. At the end of the experiment (i. e., 216 h of running and 432 PV), the removal efficiency was still up to 67%. The fixed-bed reactor showed a good performance for treating the 2,4-DCP. Due to the presence of bicarbonate, the pH of the effluent was always within an alkaline range between 8.3 and 8.6. This observation also suggests that the treating process using $CuFeS_2$ did not cause a significant pH change of solution. Fig. 8 also shows the oxidation-reduction potential (ORP) change of the effluents. The positive ORP values higher than 200 mV indicated the oxidizing capability of the system. Along with the running of fixed-bed reactor, the ORP value of effluent gradually decreased. The decreased ORP implied a decay of the oxidizing ability, which was in accordance with the decreased 2,4-DCP removal efficiency.

The leached Cu, Fe, and S species in the effluents during the 216 h of operation were measured. From the results shown in Table 1, it can be

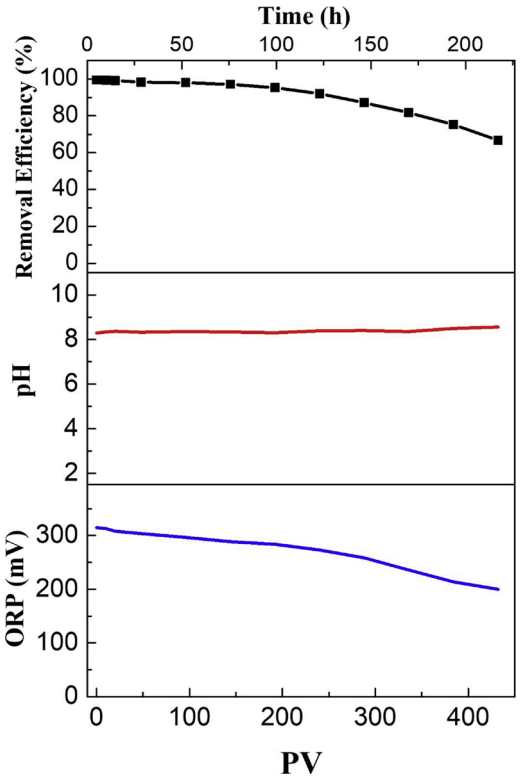

Fig. 8. Removal efficiency of 2,4-DCP, pH and ORP as a function of operation time in a fixed-bed column reactor. 70 g Al_2O_3@$CuFeS_2$ catalysts were packed in a reactor with a pore volume of 50 mL. Inlet solution consisting of 10 mg/L 2,4-DCP, 15 mM $NaHCO_3$ and 30 mM H_2O_2 was pumped into the reactor with a flow rate 100 mL/h (30 min retention time).

Table 1
Concentration of Cu, Fe and S in the effluents of column experiments.

Time	Cu (mg/L)	Fe (mg/L)	Total S (mg/L)
72 h	0.94	< 0.01	4.66
144 h	0.56	< 0.01	2.44
216 h	0.45	< 0.01	1.66

observed that the concentrations of dissolved copper species were constantly lower than 1 mg/L. According to the Chinese standard for groundwater quality (GB/T 14848-2017), these values were lower than the permissible limit of category IV groundwater (≤1.5 mg/L). The concentrations of dissolved iron species were always lower than the detection limitation (0.01 mg/L), which was probably due to the precipitation of iron species at the alkaline pH. Both the dissolved copper and iron species were within the acceptable level without notable environmental risk. As the operation progressed, the concentrations of leached copper, iron and sulphur species showed a decreasing trend. This is due to the runoff of the $CuFeS_2$ catalysts from the surface of Al_2O_3 particles. Through visual inspection, the decay of the black color of the Al_2O_3@$CuFeS_2$ fillers could be observed in the fixed-bed reactor after 216 h of operation, especially for the fillers at the bottom of the reactor (see Fig. S10 in the SM). With the decrease in the remaining $CuFeS_2$, the leached amounts of copper, iron, and sulphur species accordingly decreased. The SEM analysis on the Al_2O_3@$CuFeS_2$ fillers after reaction reveals that the detachment of the $CuFeS_2$ particles resulted in the exposure of Al_2O_3 substrate (Fig. S11 in the SM); but there is no significant difference for the TEM images (Fig. S11 in the SM). The acute toxicity of the effluent after 72 h of operation was evaluated by soil dehydrogenase activity assay, and the results (Fig. S12 in the SM)

show that the dehydrogenase activity of effluent was higher than the influent due to the degradation of 2,4-DCP, but the TPF concentration is still lower than that of the bicarbonate solution, which did not pass the Al_2O_3@$CuFeS_2$ packed column. In other words, the leached copper ions and the remaining H_2O_2 (< 10 μmol/L) still posed slight toxicity on soil dehydrogenase. Overall, the flowing experiment suggested that the Al_2O_3@$CuFeS_2$ materials can be used as the fillers in fixed-bed reactor for the effective removal of 2,4-DCP. Meanwhile, the runoff of the catalysts might release elevated levels of dissolved copper in the effluents, and the risk of secondary metal contamination should be monitored if the groundwater water quality was concerned in real remedial practices.

4. Conclusions

In the present study, three metal sulfides were prepared and their performances for activating PMC were compared, and the results showed that $CuFeS_2$ was a good heterogeneous catalyst for APMC process. The reversible redox properties endowed the $CuFeS_2$ catalyst with good capability to continuously activate PMC and produce a series of intermediated reactive species, including •OH, $^1O_2$, $•O_2^-$, and $•CO_3^-$. With the assistance of these reactive species, 2,4-DCP in the aqueous solution can be effectively degraded. After 120 min of reaction, 10 mg/L 2,4-DCP could be removed by 90% at the condition of 50 mg/L $CuFeS_2$, 60 mM H_2O_2, and 25 mM $NaHCO_3$. The XPS analysis and DFT calculation suggested that the Fe(II)/Fe(III) redox couple was the catalytic active site, rather than the low valent sulphur or cuprous atom in $CuFeS_2$. We also found that the bicarbonate concentration appeared to play a more important role than the H_2O_2 concentration for the degradation of 2,4-DCP, and an increased dosage of $CuFeS_2$ greatly improved the degradation rate of 2,4-DCP. In the flowing experiment using fixed-bed reactor, the Al_2O_3@$CuFeS_2$ fillers showed a strong capability to catalyze the PMC, and a complete removal of 2,4-DCP (> 99%) could be achieved at the initial stage of a long-term running. The leached Cu, Fe, and S species in the effluents were constantly at a low level. Overall, this study demonstrated an innovative and effective H-APMC system without the use of cobalt-based catalysts. The $CuFeS_2$-activated PMC process is expected to be developed as an environmentally friendly technology for decontamination under near-neutral pH conditions, for example, for the remediation of organic-contaminated groundwater in karst regions.

Acknowledgements

This work has been financially supported by the Natural Science Foundation of China (No. 51778505, 51709011), and the international cooperative grant from the Department of Science and Technology, Hubei Province (2018AHB016). All the DFT calculations were performed on the TianHe-2 supercomputer (LvLiang Cloud Computing Center, China).

Appendix A. Supplementary data

Supplementary material related to this article can be found, in the online version, at doi:https://doi.org/10.1016/j.apcatb.2019.03.080.

References

[1] C. Liang, H.-W. Su, Ind. Eng. Chem. Res. 48 (2009) 5558–5562.
[2] A. Tsitonaki, B. Petri, M. Crimi, H. MosbÆK, R.L. Siegrist, P.L. Bjerg, Crit. Rev. Environ. Sci. Technol. 40 (2010) 55–91.
[3] Y. Yang, J.J. Pignatello, J. Ma, W.A. Mitch, Water Res. 89 (2016) 192–200.
[4] C.M. Kao, K.D. Huang, J.Y. Wang, T.Y. Chen, H.Y. Chien, J. Hazard. Mater. 153 (2008) 919–927.
[5] A.C. Pierpoint, C.J. Hapeman, A. Torrents, Chemosphere 50 (2003) 1025–1034.
[6] Y.J. Jiang, J. Contam. Hydrol. 152 (2013) 1–11.
[7] L.C. Roberts, S.J. Hug, T. Ruettimann, M.M. Billah, A.W. Khan, M.T. Rahman, Environ. Sci. Technol. 38 (2004) 307–315.
[8] A. Asghari Moghaddam, E. Fijani, Environ. Geol. 56 (2008) 281–287.
[9] S. Khorramfar, N.M. Mahmoodi, M. Arami, H. Bahrami, Desalination 279 (2011) 183–189.
[10] M.J. Stiff, Water Res. 5 (1971) 171–176.
[11] R. Ma, Y. Wang, Z. Sun, C. Zheng, T. Ma, H. Prommer, Appl. Geochem. 26 (2011) 884–897.
[12] Z. Cheng, W. Jinliang, P. Junbing, Y. Jun, Acta Geol. Sin. Engl. 86 (2012) 973–979.
[13] L. Zhou, W. Song, Z. Chen, G. Yin, Environ. Sci. Technol. 47 (2013) 3833–3839.
[14] D. Rubio, E. Nebot, J.F. Casanueva, C. Pulgarin, Water Res. 47 (2013) 6367–6379.
[15] A. Xu, X. Li, S. Ye, G. Yin, Q. Zeng, Appl. Catal. B: Environ. 102 (2011) 37–43.
[16] W.-L. Wong, K.-P. Ho, L.Y.S. Lee, M.-H. So, T.H. Chan, K.-Y. Wong, Appl. Catal. A : Gen. 453 (2013) 244–249.
[17] M. Luo, L. Lv, G. Deng, W. Yao, Y. Ruan, X. Li, A. Xu, Appl. Catal. A : Gen. 469 (2014) 198–205.
[18] J. Peng, H. Shi, J. Li, L. Wang, Z. Wang, S. Gao, Chem. Eng. J. 306 (2016) 484–491.
[19] L. Pi, N. Yang, W. Han, W. Xiao, D. Wang, Y. Xiong, M. Zhou, H. Hou, X. Mao, Chem. Eng. J. 334 (2018) 1297–1308.
[20] J.-M. Lin, M. Liu, Spectrochim. Acta Part A 72 (2009) 126–132.
[21] X. Li, W. Shi, Q. Cheng, L. Huang, M. Wei, L. Cheng, Q. Zeng, A. Xu, Appl. Catal. A : Gen. 475 (2014) 297–304.
[22] S. Dinda, M.G.B. Drew, R. Bhattacharyya, Catal. Commun. 10 (2009) 720–724.
[23] H.H. Monfared, V. Aghapoor, M. Ghorbanloo, P. Mayer, Appl. Catal. A: Gen. 372 (2010) 209–216.
[24] A. Jawad, X. Lu, Z. Chen, G. Yin, J. Phys. Chem. A 118 (2014) 10028–10035.
[25] Y. Zhang, H.P. Tran, X. Du, I. Hussain, S. Huang, S. Zhou, W. Wen, Chem. Eng. J. 308 (2017) 1112–1119.
[26] Z. Li, L. Mi, W. Chen, H. Hou, C. Liu, H. Wang, Z. Zheng, C. Shen, CrystEngComm 14 (2012).
[27] N. Barhoumi, H. Olvera-Vargas, N. Oturan, D. Huguenot, A. Gadri, S. Ammar, E. Brillas, M.A. Oturan, Appl. Catal. B: Environ. 209 (2017) 637–647.
[28] Y. Persson, A. Shchukarev, L. Öberg, M. Tysklind, Environ. Sci. Pollut. R. 15 (2008) 463–471.
[29] M.K. Männistö, M.S. Salkinoja-Salonen, J.A. Puhakka, Water Res. 35 (2001) 2496–2504.
[30] C. Wadia, Y. Wu, S. Gul, S.K. Volkman, J. Guo, A.P. Alivisatos, Chem. Mater. 21 (2009) 2568–2570.
[31] M.X. Wang, L.S. Wang, G.H. Yue, X. Wang, P.X. Yan, D.L. Peng, Mater. Chem. Phys. 115 (2009) 147–150.
[32] J. Hu, Q. Lu, B. Deng, K. Tang, Y. Qian, Y. Li, G. Zhou, X. Liu, Inorg. Chem. Commun. 2 (1999) 569–571.
[33] N. Yang, J. Cui, L. Zhang, X. Wei, A.N. Alshawabkeh, X. Mao, J. Chem. Technol. Biot. 91 (2016) 938–947.
[34] X. Niu, X. Xu, X. Li, J. Pan, F. Qiu, H. Zhao, M. Lan, Chem. Commun. 54 (2018) 13443–13446.
[35] Y.-H.A. Wang, N. Bao, A. Gupta, Solid State Sci. 12 (2010) 387–390.
[36] S.D. Disale, S.S. Garje, J. Comput. Theor. Nanos. 3 (2010) 80–86.
[37] M. Dopson, A.-K. Halinen, N. Rahunen, D. Boström, J.-E. Sundkvist, M. Riekkola-Vanhanen, A.H. Kaksonen, J.A. Puhakka, Biotechnol. Bioeng. 99 (2008) 811–820.
[38] W. Liu, Y. Wang, Z. Ai, L. Zhang, ACS Appl. Mater. Inter. 7 (2015) 28534–28544.
[39] D. Wu, Y. Chen, Y. Zhang, Y. Feng, K. Shih, Sep. Purif. Technol. 154 (2015) 60–67.
[40] Y. Wang, H. Sun, H.M. Ang, M.O. Tadé, S. Wang, Chem. Eng. J. 245 (2014) 1–9.
[41] H. Dong, C. Sans, W. Li, Z. Qiang, Sep. Purif. Technol. 171 (2016) 144–150.
[42] H. Dong, Z. Qiang, J. Hu, C. Sans, Chem. Eng. J. 316 (2017) 288–295.
[43] T. Kuzuya, K. Itoh, M. Ichidate, T. Wakamatsu, Y. Fukunaka, K. Sumiyama, Electrochim. Acta 53 (2007) 213–217.
[44] L.D. Partain, R.A. Schneider, L.F. Donaghey, P.S. McLeod, J. Appl. Phys. 57 (1985) 5056–5065.
[45] A. Ghahremaninezhad, D.G. Dixon, E. Asselin, Electrochim. Acta 87 (2013) 97–112.
[46] P.C.J. Graat, M.A.J. Somers, Appl. Surf. Sci. 100-101 (1996) 36–40.
[47] C. Boekema, A.M. Krupski, M. Varasteh, K. Parvin, F. van Til, F. van der Woude, G.A. Sawatzky, J. Magn. Magn. Mater. 272-276 (2004) 559–561.
[48] S.R. Hall, J.M. Stewart, Acta Crystallogr. Sect. B: Struct. Sci. 29 (1973) 579–585.
[49] C. de Oliveira, G.F. de Lima, H.A. de Abreu, H.A. Duarte, J. Phys. Chem. C 116 (2012) 6357–6366.
[50] S. Conejeros, P. Alemany, M. Llunell, Id.P.R. Moreira, Vc. Sánchez, J. Llanos, Inorg. Chem. 54 (2015) 4840–4849.
[51] J.M. Fontmorin, R.C. Burgos Castillo, W.Z. Tang, M. Sillanpää, Water Res. 99 (2016) 24–32.
[52] L. Cheng, M. Wei, L. Huang, F. Pan, D. Xia, X. Li, A. Xu, Ind. Eng. Chem. Res. 53 (2014) 3478–3485.
[53] M. Liu, L. Zhao, J.M. Lin, J. Phys. Chem. A 110 (2006) 7509–7514.
[54] S.X. Liang, L.X. Zhao, B.T. Zhang, J.M. Lin, J. Phys. Chem. A 112 (2008) 618–623.
[55] J. Li, Q. Li, C. Lu, L. Zhao, J.-M. Lin, Spectrochim. Acta A 78 (2011) 700–705.
[56] Z.D. Draganić, A. Negrón-Mendoza, K. Sehested, S.I. Vujošević, R. Navarro-Gonzáles, M.G. Albarrán-Sanchez, I.G. Draganić, Int. J. Radiat. Appl. Instrum. C Radiat. Phys. Chem. 38 (1991) 317–321.
[57] K. Djebbar, T. Sehili, P. Mazellier, J. De Laat, Environ. Technol. 24 (2003) 479–489.
[58] C.A.S. Regino, D.E. Richardson, Inorg. Chim. Acta Rev. 360 (2007) 3971–3977.
[59] A. Jawad, Y. Li, X. Lu, Z. Chen, W. Liu, G. Yin, J. Hazard. Mater. 289 (2015) 165–173.